analytical chemistry

pubs.acs.org/ac Article

Back Isomerization Kinetics of Molecular Photoswitches: Complementary Insights from Liquid Chromatography and Ion Mobility Measurements

Thomas Robert, Gwendal Henrard, Benjamin Tassignon, Ari Serez, Julien De Winter, Philippe Dugourd, Jérôme Cornil, Fabien Chirot,* and Pascal Gerbaux*

Cite This: https://doi.org/10.1021/acs.analchem.5c00560 Read Online

ACCESS | Metrics & More | Article Recommendations | Supporting Information

ABSTRACT: Storing solar energy in chemical bonds through the reversible isomerization of UV−vis absorbing molecules offers a promising approach to energy storage. These molecules form high-energy photoisomers, which can store energy if kinetically protected by a significant activation barrier against spontaneous thermal back-isomerization. In this study, we compare the back-isomerization kinetic parameters ($\Delta H^{\ddagger}$ and $\Delta S^{\ddagger}$) of model azobenzene-based photoswitches in solution with those obtained in the gas phase using an original tandem ion mobility mass spectrometer. Our findings show that the activation enthalpy is well-reproduced from the solution phase to the gas phase, whereas the activation entropy is significantly affected by the absence of solvent, revealing further different relaxation mechanisms.

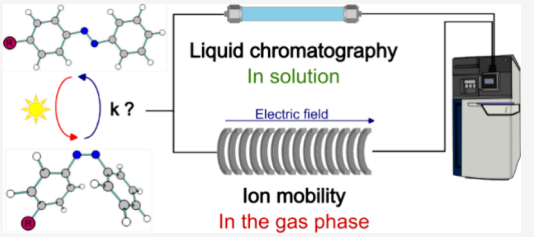

INTRODUCTION

Molecular solar thermal (MOST) systems are one of the most promising approaches for harvesting and storing solar power in chemical bonds, which can be released on-demand as thermal energy.[1,2] MOST systems exploit metastable states of molecular systems, typically stereoisomers, further referred to as photoisomers, that can be populated through light absorption. This high-energy photoisomer can store the energy difference (ΔH) between the two isomers if kinetically protected against spontaneous thermal back-isomerization by an activation barrier ($\Delta G^{\ddagger}$), i.e., the free energy difference between the high-energy photoisomer and the transition state of the thermal back-isomerization reaction.[3,4] Extensive research is conducted on various classes of chromophores to optimize their MOST properties. The key parameters that are mandatory to optimize are (i) the overlap between the solar spectrum and the absorption spectrum of the isomer in its ground state, (ii) the energy storage density (in terms of kJ kg^{-1}) that is directly related to the enthalpy difference (ΔH) between the two isomers in the ground state,[3,4] and (iii) the half-life time of the metastable isomer, which is entirely controlled by the temperature and the characteristics of the transition state of the back-isomerization reaction.[3,4]

Azobenzenes (AZO) are a particularly appealing class of MOST candidates because of their high cyclability and synthetic versatility. They exhibit a reversible photoisomerization between the stable and the metastable isomer, which corresponds to the *E* and *Z* configurations of the N=N bond, respectively (see Figure 1a).[5] However, the properties of pristine azobenzene must be improved to meet the criteria for an efficient MOST system. First, the maximum absorption of *E*-azobenzene, approximately 320 nm, does not optimally align with the solar spectrum.[5] Additionally, the half-life times of the metastable isomers on the order of 4 days at 298 K in *n*-heptane should be tuned depending on the targeted applications, e.g., for overnight vs long-term solar energy storage.[5−8] Current efforts toward the design of efficient AZO-based systems include synthetic modifications of the azobenzene core; for instance, replacing one aryl ring with a heteroaryl ring leads to switches absorbing in the visible with thermal $t_{1/2}$ ranging from days to years.[9] Grafting AZO photoswitches along a polymer backbone emerges as a strategy to significantly increase the storage energy per AZO molecule because of chemical and geometric interactions (i.e., cooperative effects).[10] Recently, we introduced peptoids as programmable supramolecular scaffolds to improve the energy storage properties of AZO-based MOST systems (see Figure 1b).[11] We demonstrated experimentally and theoretically that the dynamics of the MOST systems can be tuned based on the relative anchoring positions of the photochromic units along the peptoid backbone.[11]

Accurately determining the kinetics of the thermal back-isomerization reaction nevertheless represents a significant challenge. We recently introduced LC-MS as an original

Received: January 24, 2025
Revised: April 11, 2025
Accepted: April 14, 2025

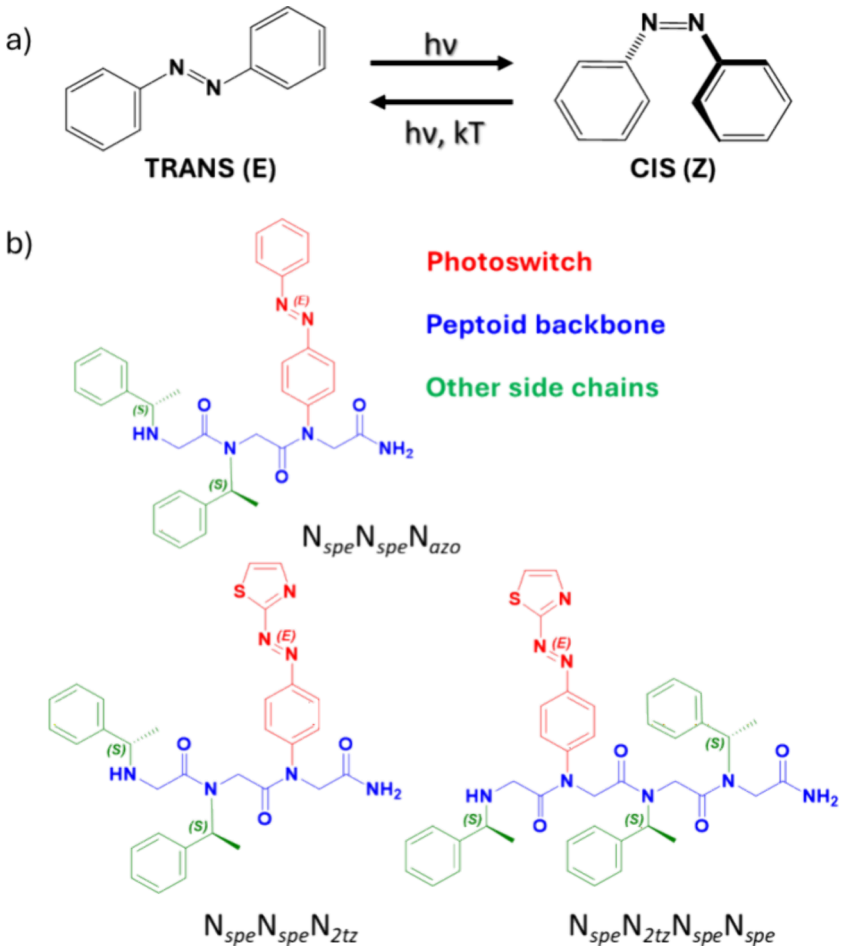

Figure 1. (a) Photoisomerization and back isomerization of azobenzene; (b) selected peptoids as MOST candidates, with (*S*)-1-phenylethyl, unsubstituted azobenzene, and 2-thiazole substituted azobenzene as side chains, denoted as N_{spe}, N_{azo}, and N_{2tz}, respectively. Peptoids are named from the N- to the C-terminal unit according to literature recommendations.[12]

method to determine the thermal back isomerization kinetics by monitoring the time evolution of the relative populations of photoisomers.[11] This involves repeated LC-MS measurements over time while keeping the freshly irradiated AZO-peptoid solutions in the HPLC autosampler, in the dark, at controlled temperatures. In principle, temperature-dependent kinetics measurements allow one to derive values for the enthalpic ($\Delta H^{\ddagger}$) and entropic ($\Delta S^{\ddagger}$) components of the activation barrier based on Eyring formalism (see SI1), and to gain a deep insight into the back isomerization kinetics. However, the limited temperature range (10−40 °C) accessible, combined with the typical LC time scale (~10 min), defines the time window accessible for monitoring the back isomerization reactions. On the one hand, slow thermal back-isomerization ($t_{1/2}$ > weeks) monitoring requires (i) a huge amount of solvent and (ii) stable experimental conditions over a long period of time, which are detrimental to measurement cost-effectiveness and reliability. On the other hand, fast reactions (<5 min) cannot be monitored using the LC-MS method. In addition, the accessible temperature range, limited to a few dozen Kelvin, further hampers the precision on the measured values as soon as extrapolation is required. Ion mobility spectrometry (IMS) separation coupled to mass spectrometry (MS) detection is nowadays more and more documented in the context of stereoisomer distinction, including photo-isomers.[13−15] The core principle of IMS is to separate gas-phase ions in an inert gas under the influence of an electric field. The ions, e.g., (stereo)isomer ions, are separated according to their ion mobility, which correlates with their speed of travel through the cell. IMS monitoring of the photoisomer ions relative proportions may be envisaged as an efficient technique complementing the LC-MS method to study back isomerization processes over time.[16]

In the present paper, we will combine gaseous ion thermal activation and ion mobility separation to determine the kinetics parameters of the gas phase *Z*-to-*E* reaction on original peptoid-grafted azobenzene derivatives (see Figure 1b). This selection of structures is driven by several considerations: (i) we recently reported that AZO-grafted peptoids are promising MOST candidates,[11] (ii) the presence of a secondary amine at the N-terminal extremity affords a basic site prone to catch the H^+, thus protecting the chromophore from ionization,[17] (iii) the thiazole-containing chromophore will red-shift the absorbance closer to the maximum of the solar spectrum, and (iv) the 4-residue peptoid is introduced to examine the influence of the chain length on the back isomerization kinetics, both in solution and in the gas phase. We will exploit a unique home-built IMS-trap-IMS tandem ion mobility instrument to characterize the transition state associated with the thermal $Z \rightarrow E$ isomerization, i.e., measure $\Delta H^{\ddagger}$ and $\Delta S^{\ddagger}$.[18,19] The kinetic parameters measured

https://doi.org/10.1021/acs.analchem.5c00560
Anal. Chem. XXXX, XXX, XXX−XXX

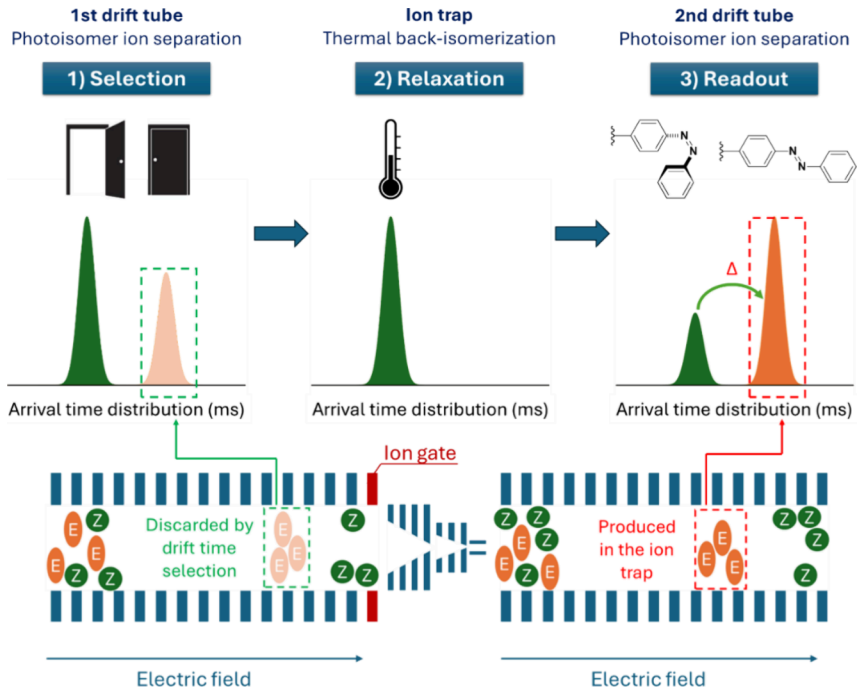

Figure 2. Principle of tandem-IMS experiments. The first drift tube separates the ionized photoisomers based on their arrival time distribution (ATD). Metastable isomer ions are selected by an ion gate that opens within their specific drift time. These ions are then stored in an ion trap and heated at a specified temperature for a set trapping time. Subsequently, the ions are ejected toward the second drift tube where the photoisomers are separated and sampled. See Figure SI6 for a schematic of the tandem-IMS instrument.

in the gas phase will then be compared to the parameters measured in methanolic solutions by our LC-MS method.

EXPERIMENTAL SECTION

To define the peptoid structure, we will use the abbreviation reported in the literature.[12] The sequence is always given from the N- to the C-terminal end, and N_{azo}, N_{2tz}, and N_{spe}, respectively, denote azobenzene, 4-[(1,3-thiazol-2-yl)-diazenyl]aniline, and (*S*)-1-phenylethyl residues. All reactants and solvents were commercially available (VWR Chemicals) and used without any further purification, except 4-[(1,3-thiazol-2-yl)diazenyl]aniline and all peptoids, whose synthesis and characterizations are described in the Supporting Information section (see SI2–4).

1° LC-MS Method To Study Thermal Kinetics in Solution. The kinetic study of the thermal back-isomerization reaction is performed by sampling the photoisomer population over time using liquid chromatography coupled with mass spectrometry. The separation by liquid chromatography is achieved using an Acquity UPLC H-Class (Waters, UK), equipped with a nonpolar ACQUITY UPLC BEH C18 column (2.1 × 50 mm; 1.7 μm) at 30 °C. The eluant follows a linear gradient starting from 70% H_2O (with 0.01% HCOOH)/30% acetonitrile (ACN), going to 100% ACN in 10 min. HPLC grade solvents were used. Photoisomers are mostly detected as $[M + H]^+$ ions by mass spectrometry using a Synapt G2-Si mass spectrometer (Waters, UK) equipped with an Electrospray ionization source operating in positive ionization mode. Samples are dissolved in methanol HPLC grade (ca. 3 × 10^{-6} M) and irradiated with either an LightningCure LC8 L9588-02A Hg–Xe lamp (Hamamatsu Photonics K.K., Hamamatsu, Japan) further equipped with an UV transmitting filter (50 × 50 mm center wavelength = 325 nm, OptoSigma) for the $N_{spe}N_{spe}N_{azo}$ and $N_{spe}N_{azo}N_{spe}$peptoids or a LightningCure LC8 L9588-03 Xe lamp (Hamamatsu Photonics K.K., Hamamatsu, Japan) for visible irradiation of the $N_{spe}N_{spe}N_{2tz}$ and the $N_{spe}N_{2tz}N_{spe}N_{spe}$ peptoids to trigger (partial) photoisomerization with an irradiance of about 1750 mW cm^{-2} for both lamps. Absorption spectra of selected azo-based and azothiazole-based peptoids are represented in Section SI5.

The autosampler chamber of the Acquity UPLC H-Class (Waters, UK) allows for conserving chromophore solutions in the dark at controlled temperature. The extent of the *Z*-to-*E* back isomerization at a given temperature is detected upon liquid chromatography separation. The extracted ion current of the protonated peptoids, including all the isotopic compositions, is integrated using homemade Python scripts, giving access to the proportion of the Z and E isomers.

2° Tandem IMS Method To Study Thermal Kinetics in the Gas Phase. The rapid study of the thermal relaxation of isolated gaseous photoisomeric ions is made possible by an original tandem ion mobility instrument (Institut Lumière-Matière, Université Lyon 1) featuring an IM-trap-IM configuration, as shown in Figures 2 and SI6.[19] Here, the temperature of the trap cell may be varied, and the residence time of the trapped ions may be adjusted to allow thermal isomerization of the trapped ions in the gas phase. In this configuration, after daylight irradiation in solution and ESI ionization, the generated metastable photoisomer ions are time-selected by the first IM cell (He as the drift gas, 4 mbar). The ions are then trapped and thermalized at a given temperature in the trapping cell (He as the buffer gas, 4.5 mbar) for a controlled duration (from 1 μs to several seconds), allowing the relaxation process to occur. All ions are then ejected toward the second IM cell (He as the drift gas, 4 mbar), where they are separated according to their *Z*/*E* configuration.

https://doi.org/10.1021/acs.analchem.5c00560
Anal. Chem. XXXX, XXX, XXX−XXX

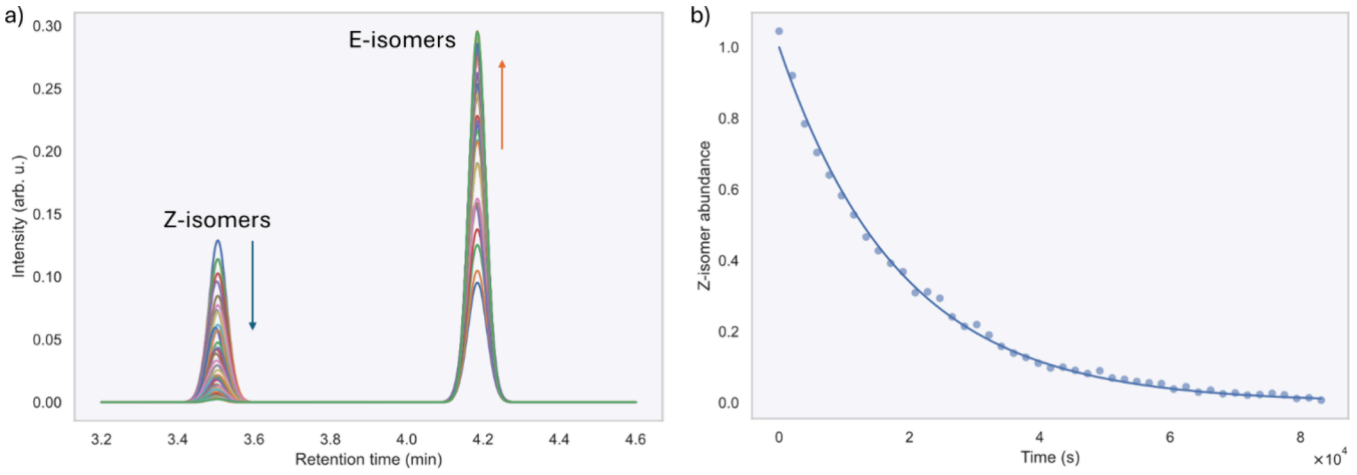

Figure 3. (a) *Z*- and *E*-isomer separation of the $N_{spe}N_{spe}N_{2tz}$ system by LC-MS over time at 20 °C. (b) *Z*-isomer relative abundance is then plotted against time and fitted by a mono exponential decay fit $R^2 = 0.997$.

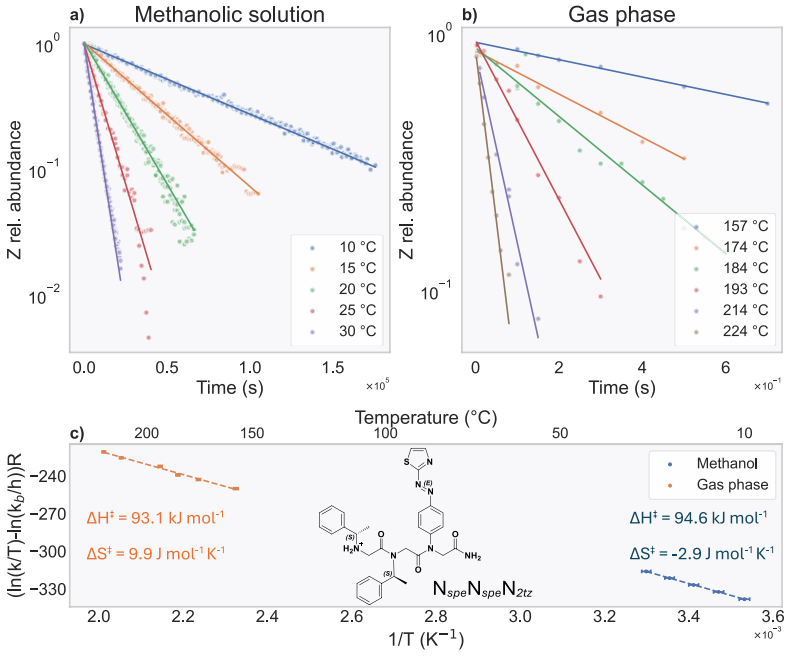

Figure 4. (a) Solution kinetics for the $N_{spe}N_{spe}N_{2tz}$ system in methanol showing the evolution of the *Z* photoisomer relative abundance over time in the dark at the specified temperatures. (b) Gas-phase kinetics for the $N_{spe}N_{spe}N_{2tz}$ system. *Z* photoisomer relative abundances are fitted by a monoexponential decay (solid lines) from which the kinetic constant *k* of the back-isomerization reaction is derived for each temperature in solution and the gas-phase (see SI1). (c) Eyring plots corresponding to the k obtained at each temperature in solution (blue) and in the gas-phase (orange). The apparent activation parameters $\Delta H^{\ddagger}$ and $\Delta S^{\ddagger}$ are extracted from the slope and the intercept of the linear fits (dashed lines), respectively (see SI1).

The ions are detected by a modified Maxis Impact QToF mass spectrometer (Bruker Daltonik, Bremen, Germany). Rate constants are extracted from the evolution of the relative intensities of the *Z* and *E* isomers as a function of the trapping time in the thermalized cell using homemade Python scripts (see SI1). The procedure is repeated at different trapping temperatures to obtain temperature-dependent decay rates.

RESULTS AND DISCUSSION

Methanolic solutions of the three selected peptoids are exposed to light irradiation (see the Experimental Section) until a steady state is reached to maximize the *Z*-photoisomer population available for both the solution phase and gas phase experiments. The irradiated solutions are then immediately used for the LC-MS investigations or the tandem IMS experiments to generate the kinetic parameters for the solution and gas phase *Z*-to-*E* back isomerization, respectively.

1° LC-MS Determination of the Thermal Kinetics in Solution. Both *Z* and *E* photoisomers of the three peptoids are baseline separated upon LC separation, as featured in Figure SI7, and are mostly detected as $[M + H]^+$ ions. By LC-MS signal integration, the relative proportion of the metastable photoisomers can be accessed over time (Figure 3a). The kinetics of the $Z \rightarrow E$ thermal relaxation is attributed to first-order kinetics, as confirmed by the excellent fit to a first-order exponential decay model, as exemplified in Figure 3b.

https://doi.org/10.1021/acs.analchem.5c00560
Anal. Chem. XXXX, XXX, XXX−XXX

Table 1. Determination of the Kinetics Parameters Using LC-MS Experiments (a) and Gas Phase Back Isomerization Using Tandem-IMS Experiments (b) of the Three Selected Peptoids[1,a]

a)

Peptoid sequence	$\Delta H_{Eyring}^{\ddagger}$ in solution (kJ mol^{-1})	$\Delta S_{Eyring}^{\ddagger}$ in solution (J mol^{-1} K^{-1})	$\Delta G_{Eyring}^{\ddagger}$ (293 K) in solution (kJ mol^{-1})	$t_{1/2}$ (293 K) in solution
$N_{spe}N_{spe}N_{azo}$	96.8[1]	-34[1]	106.7	14 d
$N_{spe}N_{spe}N_{2tz}$	94.9 ± 0.3	-2.9 ± 1.1	95.8 ± 0.6	4 h
$N_{spe}N_{2tz}N_{spe}N_{spe}$	100.0 ± 1.6	16.2 ± 5.5	95.2 ± 3.2	3 h

b)

Peptoid sequence	Ions	$\Delta H_{Eyring}^{\ddagger}$ Gas phase (kJ mol^{-1})	$\Delta S_{Eyring}^{\ddagger}$ Gas phase (J mol^{-1} K^{-1})	$\Delta G_{Eyring}^{\ddagger}$ (293K) Gas phase (kJ mol^{-1})	$t_{1/2}$ (293 K) Gas phase
$N_{spe}N_{spe}N_{azo}$	$[M + H]^+$	101.6 ± 1.8	-25.4 ± 0.5	109.0 ± 1.9	36 ± 27 d
	$[M + Na]^+$	98.1 ± 0.9	-32.9 ± 0.3	107.9 ± 1.0	21 ± 8 d
$N_{spe}N_{spe}N_{2tz}$	$[M + H]^+$	93.1 ± 0.5	9.85 ± 0.05	90.2 ± 0.5	23 ± 5 min
$N_{spe}N_{2tz}N_{spe}N_{spe}$	$[M + H]^+$	91.7 ± 2.2	-41.6 ± 1.1	103.8 ± 2.5	4 ± 4 d

[a] $\Delta H_{Eyring}^{\ddagger}$, $\Delta S_{Eyring}^{\ddagger}$, $\Delta G_{Eyring}^{\ddagger}$ (293 K), and $t_{1/2}$ (293 K) are, respectively, the activation enthalpy, entropy, and Gibbs free energy, and the metastable isomer half-life time (min, d and h stand for minutes, days and hours. Data from ref 11.

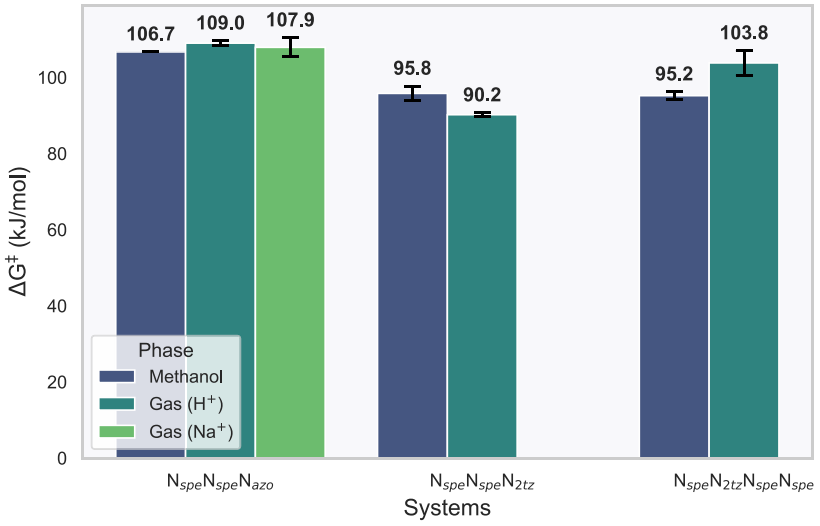

Figure 5. Activation free Gibbs energies at 293 K (see also Table 1) for the solution and gas-phase systems (protonated molecules for all systems and ionized with a sodium ion for $N_{spe}N_{spe}N_{azo}$).

This model effectively describes the decrease in the population of metastable photoisomers, allowing the rate constant to be extracted (Figure 4a,b). By measuring kinetic constants k at different temperatures T and plotting $\ln(k/T)$ as a function of the inverse of the temperature $1/T$ (Figure 4c), the activation enthalpic $\Delta H_{Eyring}^{\ddagger}$ and entropic $\Delta S_{Eyring}^{\ddagger}$ components of the thermal back-isomerization can be determined (see Table 1).

As shown in Table 1 and displayed in Figure 5, when replacing a pristine azobenzene unit with a 2-thiazole substituted derivative on the C-terminal position of a three-unit peptoid ($N_{spe}N_{spe}N_{azo}$ → $N_{spe}N_{spe}N_{2tz}$), the activation enthalpy remains roughly the same, but we observe a sharp increase of about 30 J mol^{-1} K^{-1} for the activation entropy, leading to a huge drop of the half-life time (methanol, 293 K) of the metastable isomers, from 14 days ($N_{spe}N_{spe}N_{azo}$) to 4 h ($N_{spe}N_{spe}N_{2tz}$). The kinetic parameters of the 4-unit peptoid, i.e., $N_{spe}N_{2tz}N_{spe}N_{spe}$, are also gathered in Table 1 and Figure 5, exhibiting both the highest activation enthalpy and entropy among all studied systems in methanol, and thus resulting in the lowest half-life time at 293 K due to the entropy contribution. Indeed, while the increase in activation enthalpy is slight (3% higher compared to the $N_{spe}N_{spe}N_{azo}$ system), the activation entropy sharply increases, reaching a positive value of ∼16 J mol^{-1} K^{-1} to be compared to −2.9 J mol^{-1} K^{-1} for the three-unit thiazole system.

2° Tandem-IMS Determination of the Thermal Kinetics in the Gas Phase. Upon ESI analysis, $[M + H]^+$ and $[M + Na]^+$ ions are formed for the three selected peptoids, i.e., $N_{spe}N_{spe}N_{azo}$, $N_{spe}N_{spe}N_{2tz}$, and $N_{spe}N_{2tz}N_{spe}N_{spe}$. Due to the presence of the N-terminal secondary amine and the acidic cleavage used to release the peptoids from the Rink resin, the

https://doi.org/10.1021/acs.analchem.5c00560
Anal. Chem. XXXX, XXX, XXX−XXX

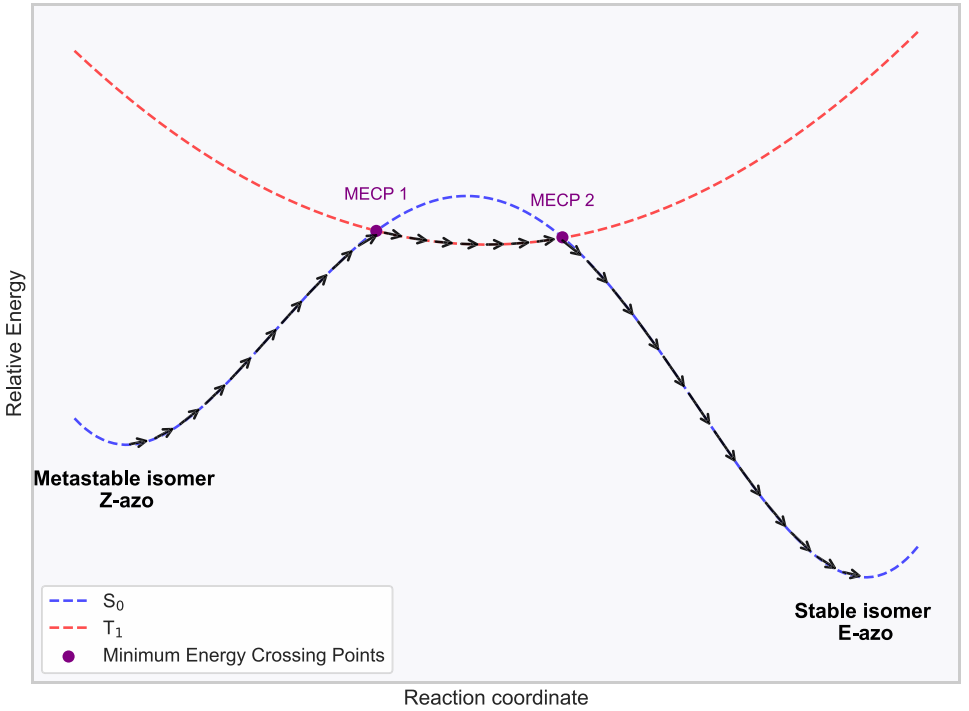

Figure 6. Energy diagram as a function of the reaction coordinate representing type II rotation for the thermal back-isomerization process (pathway indicated by arrows) for an azo-based system passing from the ground state S_0 (in blue) to the triplet state T_1 (in red) via the two minimum energy crossing points, MECPs.

three peptoids are likely to be predominantly protonated in the polar solution phase. To allow for a direct comparison between the solution and gas phase kinetic data, we will focus primarily on the gaseous $[M + H]^+$ ions but will also consider the $[M + Na]^+$ ions of $N_{spe}N_{spe}N_{azo}$ to figure out the putative impact of the cationizing agent on the gas phase kinetic parameters.

As shown in Figure SI9, all ionized *E*- and *Z*-photoisomers of the three peptoids are nicely time-resolved upon IMS, which is the prerequisite of the experiments. All ions are then subjected to tandem-IMS experiments to determine the gas-phase thermal back-isomerization kinetics of the ionized *Z*-photoisomers. The thermal back-isomerization kinetics for all the investigated ions are gathered in Table 1b and Figure 5. As shown in Figure 4b, the decay of the *Z*-photoisomer population is well fitted by first-order exponential decay kinetics (see Figure 3, for example, with LC separation). Given the high temperatures used, the gas-phase relaxation times for the thermal back-isomerization process are in the millisecond time frame. Measurements of kinetics in the gas phase are therefore faster and less resource-consuming, although slightly less precise, because of the lower number of experimental points than in methanol. As it was done in solution, the kinetic constants extracted from the exponential decay fits at each temperature (see SI1) are represented in an Eyring plot in Figure 4c, which also shows the complementarity in temperature ranges between the LC-MS (in solution) and tandem-IMS (in the gas-phase) methods.

From Table 1 and Figure 5, the activation parameters measured in the gas phase for the system $[N_{spe}N_{spe}N_{azo} + H]^+$ appear slightly different from the methanol data for the activation enthalpies (96.8 (MeOH) vs 101.6 (vacuum) kJ mol^{-1}). However, the difference in activation entropies is more significant (−34 vs −25.4 J mol^{-1} K^{-1} ; $\Delta\Delta G^{\ddagger} \sim 3$ kJ mol^{-1} at 293 K), but the entropy values remain negative. When considering the $[N_{spe}N_{spe}N_{azo} + Na]^+$ ions, the solution phase and gas phase data are remarkably in line with $\Delta H_{Eyring}^{\ddagger} = 96.8$ vs 98.1 kJ mol^{-1} and $\Delta S_{Eyring}^{\ddagger} = -34$ vs −32.9 J mol^{-1} K^{-1}, respectively, for the condensed vs gas phase conditions. In the case of the $[N_{spe}N_{spe}N_{2tz} + H]^+$ ions, the activation enthalpy is nicely conserved on going from the condensed to the gas phase (95.1 vs 93.1 kJ mol^{-1}), whereas the activation entropy undergoes variation from −2.3 to 9.9 J mol^{-1} K^{-1}. For the longer peptoid ions, $[N_{spe}N_{2tz}N_{spe}N_{spe} + H]^+$ ions, both the activation enthalpies and entropies are significantly different going from the solution to the gas phase with $\Delta H_{Eyring}^{\ddagger} = 100.0$ vs 91.7 kJ mol^{-1} and $\Delta S_{Eyring}^{\ddagger} = 16.2$ vs −41.6 J mol^{-1} K^{-1}, respectively. Note that, besides the addition of one N_{spe} residue compared to the 3-unit peptoids, the position of the chromophore in the 4-unit peptoid backbone is also different. The solvent reorganization could also affect both the activation enthalpies and entropies. Moreover, the condensed phase measurements are only performed here in methanol, a polar protic solvent, for solubility reasons, whereas the MS environment is a gas-phase system with minimal solvation effects, which can be described as an apolar medium, impacting therefore the energy barrier toward the transition state.

On the one hand, the free Gibbs activation energies at 293 K of the gas phase kinetics (see Table 1b) match well with the methanolic values for the pristine azobenzene system, both cationized with a proton and a sodium ion. On the other hand, for the $N_{spe}N_{spe}N_{2tz}$ system, the value is too low compared with the solution phase value of $\Delta G^{\ddagger}$ (293 K) but still ranks well against the values of the pristine azobenzene system. However, the free Gibbs activation energy for the four-unit peptoid bearing a thiazole-substituted azobenzene is overestimated when compared to that of the three-unit peptoid due to the large change in activation entropy observed.

https://doi.org/10.1021/acs.analchem.5c00560
Anal. Chem. XXXX, XXX, XXX−XXX

3° Thermal Back-Isomerization Pathway. In fact, the extremely low (negative) activation entropy observed in certain systems is a well-documented phenomenon, referred to as the "entropy puzzle".[20] This phenomenon is comprehensively discussed by Reimann et al., who attributed it to the actual mechanism of the thermal back-isomerization reaction.[21] The photoisomerization $E \rightarrow Z$ pathway of azobenzene has been extensively investigated, with the accepted mechanism described as inversion-assisted by rotation, i.e., lying between a pure inversion of the nitrogen configuration and a pure rotation of the N=N double bonds.[22] On the other hand, the thermal back-isomerization mechanism has been less studied, and an inversion mechanism is commonly accepted. However, Cembran et al. have recently proposed that this process rather follows a multistate pathway involving an intersystem crossing to the T_1 state, which becomes lower in energy than the S_0 state around the transition state reaction coordinates.[23] This process, enabled by the spin−orbit coupling, is associated with a rotation mechanism around the −N=N− bond passing through an orthogonal arrangement of the phenyl rings. In such a type II rotation (rotation accompanied by an intersystem crossing), there is no transition state but rather two minimum energy crossing points (MECPs) allowing for the transitions from S_0 to T_1 and from T_1 to S_0 as shown in Figure 6. To describe the kinetics of thermal back-isomerization in this scenario, it is essential to consider the spin−orbit coupling dependence on the Eyring transmission coefficient, as outlined by Liu et al. based on the Wentzel−Kramers−Brillouin theory.[24] The kinetics of thermal back-isomerization reactions that transition via the T_1 state are characterized by apparent activation parameters, namely $\Delta\tilde{H}^{\ddagger}$ and $\Delta\tilde{S}^{\ddagger}$, which account for the impact of this transmission coefficient, γ, in the Eyring equation (see SI1). In the case of a temperature-independent γ, while the activation enthalpy and the apparent activation enthalpy are quasi equivalent, the activation entropy is significantly altered, as shown in eq 1.[21] When $\gamma = 1$, $\Delta\tilde{S}^{\ddagger} = \Delta S^{\ddagger}$, and the reaction occurs by crossing the transition state in S_0. Transiting to the T_1 state via a small spin−orbit coupling, $\gamma \ll 1$, results in a highly negative apparent entropy of activation, as exemplified by the value measured for $N_{spe}N_{spe}N_{azo}$ (−34 J mol^{-1} K^{-1}), which is consistent with a rotation mechanism involving an intersystem crossing (ISC) process.

$$\Delta\tilde{S}^{\ddagger} = \Delta S^{\ddagger} + R\ln(\gamma) \quad (1)$$

The proposed multistate process offers a clearer understanding of the differences in kinetic rates between the azobenzene and thiazole-based systems, i.e., more than 30 J mol^{-1} K^{-1} in the measured activation entropies, which is especially appealing and could suggest different relaxation mechanisms involving or not an ISC. Note that a 30 J mol^{-1} K^{-1} difference in activation entropy at 293 K corresponds approximately to a drop of 8.8 kJ mol^{-1} in the activation Gibbs free energy of the thermal back-isomerization reaction. The $N_{spe}N_{spe}N_{azo}$ system exhibits activation parameters that closely align with those determined computationally by Riemann et al. for pristine azobenzene, with $\Delta\tilde{H}^{\ddagger} = \Delta H_{Eyring}{}^{\ddagger}$ and $\Delta\tilde{S}^{\ddagger} = \Delta S_{Eyring}{}^{\ddagger}$ values of 95 kJ mol^{-1} and −38 J mol^{-1} K^{-1}, respectively, that were found to be consistent with experimental results in *n*-hexane.[21] Given the presence of heavy atoms in the thiazole unit, which increases the spin−orbit coupling magnitude, the entropy of activation is expected to be higher. This is because the transmission coefficient increases with spin−orbit coupling, facilitating the transition from the S_0 to the T_1 state, which is the rate-limiting step of the thermal back-isomerization process in the type II rotation mechanism. While the possibility of an ISC process has also been theoretically proposed for azothiophenes,[25] inducing the experimentally observed difference of about 30 J mol^{-1} K^{-1} would require that the Eyring transmission coefficient needs to be increased by around 40 times. Such an increase seems inconsistent given the evolution of the transmission coefficient with the magnitude of the spin−orbit coupling (see Figure SI10).

To explain the significant difference in activation entropy for the thiazole systems, we hypothesized that the thermal back-isomerization process follows an inversion mechanism that remains in the S_0 state. This conclusion seems consistent with calculations performed by Singer et al., which pointed out that phenylazo-1,3,5-trimethylpyrazole (PATP) thermal back-isomerization results from two pathways with 75% aryl ring inversion and 24% of type II rotation although the different nature of the chromophore and the presence of the peptoid structure are expected to impact the back-isomerization.[26] This variation in the mechanism pathway, therefore, likely arises from the substitution of the aryl ring by a thiazole group. When considering that only S_0 is involved for thermal back-isomerization, the calculations yield an apparent activation entropy for the inversion mechanism of 11 J mol^{-1} K^{-1},[21] significantly increased compared to $N_{spe}N_{spe}N_{azo}$ and in line with the measured value for the $N_{spe}N_{spe}N_{2tz}$ system both in methanol and in the gas-phase. As demonstrated by Riemann et al., external heavy elements (e.g., iodide ions in solution) amplify spin−orbit coupling, increasing both the apparent activation entropy and the rate of thermal back-isomerization of pristine azobenzene, which follows a type II rotation. Using our LC-MS method, we measured the thermal back-isomerization kinetics for two peptoids, one with pristine azobenzene and the other with a thiazole derivative, in the presence of ammonium iodide salt (see Figures SI11 and SI12). The results displayed in Table 2 show distinct pathways for the two photoswitches. Indeed, for the pristine azobenzene-based peptoid, the rate of thermal back-isomerization is increased by about four times with 100 equiv of NH_4I at 303 K, in line with the kinetics measurement of pristine azobenzene in solution in the presence of tetra-*n*-butylammonium iodide.[21] This indicates that the type II rotation mechanism is conserved in the three-unit peptoid with *S*-phenylethyl side chains.

Table 2. Kinetics of the Thermal Back-Isomerization of Two Three-Unit Peptoids, $N_{spe}N_{azo}N_{spe}$ and $N_{spe}N_{spe}N_{2tz}$, Respectively, with a Pristine and a Thiazole-Substituted Azobenzene, without and with the Addition of Ammonium Iodide[a]

	$N_{spe}N_{azo}N_{spe}$ kinetic constant at 303 K (s^{-1})	$N_{spe}N_{spe}N_{2tz}$ kinetic constant at 293 K (s^{-1})
methanol	(3.7 ± 0.5) × 10^{-6}	(5.4 ± 0.1) × 10^{-5}
100 eq NH_4I in methanol	(1.4 ± 0.1) × 10^{-5}	(5.2 ± 0.1) × 10^{-5}

[a]The kinetic constants and their error are extracted from an exponential decay fitting function of the evolution of *Z*-isomer population over time (see SI9). Note that compared to the precedent data (see Table 1), $N_{spe}N_{spe}N_{azo}$ is here replaced by $N_{spe}N_{azo}N_{spe}$ for practical reasons related to the 14-day half-life time of the metastable *Z*-azo switch when positioned at the C_{ter} of the peptoid

https://doi.org/10.1021/acs.analchem.5c00560
Anal. Chem. XXXX, XXX, XXX−XXX

External iodide ions do accelerate the intersystem crossing rate from the S_0 to the T_1 states, characteristic of this mechanism. In contrast, the 2-thiazole-substituted azobenzene shows no significant change in thermal back-isomerization kinetics, with or without ammonium iodide at 20 °C (Table 2). This strongly suggests that the back-isomerization mechanism of the thiazole derivative bypasses the triplet T_1 state and rather follows an inversion mechanism, consistent with the measured apparent entropies of activation.

Therefore, we can conclude that the system $N_{spe}N_{spe}N_{azo}$, with three units and a pristine azobenzene as photoswitching unit, undergoes thermal back-isomerization reaction via an intersystem type II rotation mechanism both in solution and in the gas phase. The apparent activation entropies measured in both media (Table 1) are very close to each other, and kinetic measurements with ammonium iodide (Table 2) highlight the critical role of the spin−orbit coupling in the relaxation kinetics. While the kinetics in solution for the system $N_{spe}N_{spe}N_{2tz}$ is not impacted by the presence of ammonium iodide, indicating an inversion mechanism for the back-isomerization, the matching of the measured apparent activation entropies indicates that again there is a conservation of the relaxation pathway between the solution and the gas phase. The four-unit system $N_{spe}N_{2tz}N_{spe}N_{spe}$, bearing also a thiazole-substituted azobenzene, exhibits more complexity in contrast with the two three-unit systems. Apparent activation entropy measurements suggest an inversion mechanism in methanol (see Table 1a) and a type II rotation in the gas phase (see Table 1b), showing a significant difference in the interactions between the *S*-phenyl side chains and the azothiazole photoswitching unit. These findings indicate that, besides the nature of the photoswitching unit and the presence of solvent, there is a complex relationship between the structure of the peptoid-based MOST systems studied and the mechanism of the thermal back-isomerization reaction.

CONCLUSIONS

Photoswitchable molecules that undergo reversible photoisomerization into long-lived metastable states hold significant potential for solar energy storage applications. The half-life times ($t_{1/2}$) of these photoisomers is a critical parameter, governed by two main kinetic factors ($\Delta H^{\ddagger}$ and $\Delta S^{\ddagger}$), which are typically estimated by following the metastable photoisomer decay over time at different temperatures. However, accurately determining the kinetics of photoisomer thermal back-isomerization remains challenging in solution, especially due to limitations in the temperature range (10−40 °C) and time range (>10 min). In this study, we successfully employed an innovative tandem ion mobility mass spectrometry approach, combining gaseous ion thermal activation and ion mobility separation, to determine the kinetic parameters of the gas phase *Z*-to-*E* isomerization of peptoid-grafted azobenzene derivatives. Our comparison of gas-phase data with solution-phase measurements, obtained by expanding our LC-MS method to new MOST systems, highlights that while activation enthalpy is quite similar in the gas phase and in solution, the actual mechanism of the thermal back-isomerization plays a key role to understand the changes in amplitude and sign of the entropic effects during the solution-to-gas-phase transition.

The pathway of the back-isomerization can either remain on the ground S_0 electronic state or transit through the triplet T_1 by an intersystem crossing, which is reflected by a largely negative apparent activation entropy $\Delta\tilde{S}$. The measurement of activation entropies in solution and in the gas-phase, coupled with kinetics data collected in the presence of NH_4I, demonstrates a strong structure dependence of the back-isomerization mechanism with (i) the pristine azobenzene system showing a type II rotation both in solution and in the gas-phase, (ii) the three-unit thiazole derivative exhibiting an inversion mechanism both in solution and in the gas phase, and (iii) the four-unit peptoid displaying an inversion in solution and a type II rotation mechanism in the gas phase.

While translating gas-phase data to solution-phase kinetics is challenging due to solvent effects on the thermal back-isomerization process, our findings suggest that gas-phase experiments can provide a rapid and efficient method for predicting and screening activation barriers. These experiments also complement solution-phase measurements by covering different temperature and time scales. However, it should be noted that LC-MS and tandem IMS techniques should not be suitable for photoswitches with very fast back-isomerization (typically <1 s), for which laser irradiation coupled to ion mobility should be more appropriate.[27]

Moving forward, we are expanding our data set across various systems, supplemented by theoretical simulations, to evaluate the correlation between gas-phase and solution-phase kinetics, and to explore the changes in the back-isomerization mechanisms between the two phases based on activation entropy values.

ASSOCIATED CONTENT

Data Availability Statement

Raw data and notebooks used to generate the figures can be found at S²MOs GitHub at https://github.com/S2MOs/KIMETICS_paper

Supporting Information

The Supporting Information is available free of charge at https://pubs.acs.org/doi/10.1021/acs.analchem.5c00560.

Description of the data treatment; system synthesis, characterization, and absorption spectra; additional experimental setup details; Eyring transmission coefficient and spin−orbit coupling relationship plot; LC-MS and tandem IMS-MS data (PDF)

AUTHOR INFORMATION

Corresponding Authors

Fabien Chirot − *Université Claude Bernard Lyon 1, CNRS, Institut Lumière Matière, F-69622 Lyon, France;* orcid.org/0000-0001-9115-9233; Email: fabien.chirot@univ-lyon1.fr

Pascal Gerbaux − *Organic Synthesis and Mass Spectrometry laboratory, University of Mons, UMONS, B-7000 Mons, Belgium;* orcid.org/0000-0001-5114-4352; Email: pascal.gerbaux@umons.ac.be

Authors

Thomas Robert − *Organic Synthesis and Mass Spectrometry laboratory, University of Mons, UMONS, B-7000 Mons, Belgium*

Gwendal Henrard − *Organic Synthesis and Mass Spectrometry laboratory and Laboratory for Chemistry of Novel Materials, University of Mons, UMONS, B-7000 Mons, Belgium*

Benjamin Tassignon − *Organic Synthesis and Mass Spectrometry laboratory and Laboratory for Chemistry of*

https://doi.org/10.1021/acs.analchem.5c00560
Anal. Chem. XXXX, XXX, XXX−XXX

Novel Materials, University of Mons, UMONS, B-7000 Mons, Belgium

Ari Serez − *Organic Synthesis and Mass Spectrometry laboratory and Laboratory for Chemistry of Novel Materials, University of Mons, UMONS, B-7000 Mons, Belgium*

Julien De Winter − *Organic Synthesis and Mass Spectrometry laboratory, University of Mons, UMONS, B-7000 Mons, Belgium;* orcid.org/0000-0003-3429-5911

Philippe Dugourd − *Université Claude Bernard Lyon 1, CNRS, Institut Lumière Matière, F-69622 Lyon, France;* orcid.org/0000-0003-4395-1140

Jérôme Cornil − *Laboratory for Chemistry of Novel Materials, University of Mons, UMONS, B-7000 Mons, Belgium;* orcid.org/0000-0002-5479-4227

Complete contact information is available at: https://pubs.acs.org/10.1021/acs.analchem.5c00560

Notes

The authors declare no competing financial interest.

■ ACKNOWLEDGMENTS

The S^2MOs and CMN laboratories are grateful to the "Fonds National de la Recherche Scientifique" (FRS-FNRS) for continuing support. J.C. is an FNRS research fellow. T.R. and B.T. thank the "Fonds pour la Recherche Industrielle et Agricole" (FRIA) for their Ph.D. grants. G.H. thanks the FNRS for his PhD grant in the frame of the PDR project T.0095.22 "AZO_MOST". A.S. thanks the UMONS for his PhD grant in the frame of the ARC project "Molecular Solar Thermal systems: from molecules to energy capture/exchange prototypes" (ARC-23/27 UMONS2). The IMS-IMS setup was developed with funding from the Agence Nationale pour la Recherche (grant no. 17-CE29-001301).

■ REFERENCES

(1) Kucharski, T. J.; Tian, Y.; Akbulatov, S.; Boulatov, R. *Energy Environ. Sci.* **2011**, *4* (11), 4449.
(2) Lennartson, A.; Roffey, A.; Moth-Poulsen, K. *Tetrahedron Lett.* **2015**, *56* (12), 1457−1465.
(3) Wang, Z.; Erhart, P.; Li, T.; Zhang, Z.-Y.; Sampedro, D.; Hu, Z.; Wegner, H. A.; Brummel, O.; Libuda, J.; Nielsen, M. B.; Moth-Poulsen, K. *Joule* **2021**, *5* (12), 3116−3136.
(4) Börjesson, K.; Lennartson, A.; Moth-Poulsen, K. *ACS Sustain Chem. Eng.* **2013**, *1* (6), 585−590.
(5) Bandara, H. M. D.; Burdette, S. C. *Chem. Soc. Rev.* **2012**, *41* (5), 1809−1825.
(6) Sun, C.; Wang, C.; Boulatov, R. *ChemPhotoChem.* **2019**, *3* (6), 268−283.
(7) Dong, L.; Feng, Y.; Wang, L.; Feng, W. *Chem. Soc. Rev.* **2018**, *47* (19), 7339−7368.
(8) Olmsted, J.; Lawrence, J.; Yee, G. G. *Sol. Energy* **1983**, *30* (3), 271−274.
(9) Weston, C. E.; Richardson, R. D.; Haycock, P. R.; White, A. J. P.; Fuchter, M. J. *J. Am. Chem. Soc.* **2014**, *136* (34), 11878−11881.
(10) Jeong, S. P.; Renna, L. A.; Boyle, C. J.; Kwak, H. S.; Harder, E.; Damm, W.; Venkataraman, D. *Sci. Rep.* **2017**, *7* (1), 17773.
(11) Tassignon, B.; Wang, Z.; Galanti, A.; De Winter, J.; Samorì, P.; Cornil, J.; Moth-Poulsen, K.; Gerbaux, P. *Chem. − Eur. J.* **2023**, *29* (70), No. e202303168.
(12) Zuckermann, R. N.; Kerr, J. M.; Kent, S. B. H.; Moos, W. H. *J. Am. Chem. Soc.* **1992**, *114* (26), 10646−10647.
(13) Markworth, P. B.; Adamson, B. D.; Coughlan, N. J. A.; Goerigk, L.; Bieske, E. J. *Phys. Chem. Chem. Phys.* **2015**, *17* (39), 25676−25688.
(14) Bull, J. N.; Carrascosa, E.; Mallo, N.; Scholz, M. S.; da Silva, G.; Beves, J. E.; Bieske, E. J. *J. Phys. Chem. Lett.* **2018**, *9* (3), 665−671.
(15) Czerwinska, I.; Kulesza, A.; Choi, C.; Chirot, F.; Simon, A. L.; Far, J.; Kune, C.; De Pauw, E.; Dugourd, P. *Phys. Chem. Chem. Phys.* **2016**, *18* (47), 32331−32336.
(16) Poyer, S.; Choi, C. M.; Deo, C.; Bogliotti, N.; Xie, J.; Dugourd, P.; Chirot, F.; Salpin, J.-Y. *Analyst* **2020**, *145* (11), 4012−4020.
(17) Halin, E.; Hoyas, S.; Lemaur, V.; De Winter, J.; Laurent, S.; Cornil, J.; Roithová, J.; Gerbaux, P. *Int. J. Mass Spectrom.* **2019**, *435* (47), 217−226.
(18) Simon, A.-L.; Chirot, F.; Choi, C. M.; Clavier, C.; Barbaire, M.; Maurelli, J.; Dagany, X.; MacAleese, L.; Dugourd, P. *Rev. Sci. Instrum.* **2015**, *86* (9), No. 094101.
(19) Le Fèvre, A.; Dugourd, P.; Chirot, F. *Anal. Chem.* **2021**, *93* (9), 4183−4190.
(20) Rietze, C.; Titov, E.; Lindner, S.; Saalfrank, P. *J. Phys.: Condens. Matter* **2017**, *29* (31), 314002.
(21) Reimann, M.; Teichmann, E.; Hecht, S.; Kaupp, M. *J. Phys. Chem. Lett.* **2022**, *13* (46), 10882−10888.
(22) Bandara, H. M. D.; Burdette, S. C. *Chem. Soc. Rev.* **2012**, *41* (5), 1809−1825.
(23) Cembran, A.; Bernardi, F.; Garavelli, M.; Gagliardi, L.; Orlandi, G. *J. Am. Chem. Soc.* **2004**, *126* (10), 3234−3243.
(24) Liu, S.; Srinivasan, S.; Tao, J.; Grady, M. C.; Soroush, M.; Rappe, A. M. *J. Phys. Chem. A* **2014**, *118* (40), 9310−9318.
(25) Heindl, A. H.; Wegner, H. A. *European Journal* **2020**, *26* (60), 13730−13737.
(26) Singer, N. K.; Schlögl, K.; Zobel, J. P.; Mihovilovic, M. D.; González, L. *J. Phys. Chem. Lett.* **2023**, *14* (40), 8956−8961.
(27) Bull, J. N.; Scholz, M. S.; Coughlan, N. J. A.; Kawai, A.; Bieske, E. J. *Anal. Chem.* **2016**, *88* (24), 11978−11981.